Grating design for the Water Recovery X-ray Rocket

Drew M. Miles, Randall L. McEntaffer, Benjamin D. Donovan, James H. Tutt, Tyler Steiner, et al.

Drew M. Miles, Randall L. McEntaffer, Benjamin D. Donovan, James H. Tutt, Tyler Steiner, Christopher R. Hillman, Jake A. McCoy, Ningxiao Zhang, "Grating design for the Water Recovery X-ray Rocket," Proc. SPIE 10699, Space Telescopes and Instrumentation 2018: Ultraviolet to Gamma Ray, 106996K (6 July 2018); doi: 10.1117/12.2312648

SPIE.

Event: SPIE Astronomical Telescopes + Instrumentation, 2018, Austin, Texas, United States

Grating design for the Water Recovery X-ray Rocket

Drew M. Miles[a], Randall L. McEntaffer[a], Benjamin D. Donovan[a], James H. Tutt[a], Tyler Steiner[b], Christopher R. Hillman[a], Jake A. McCoy[a], and Ningxiao Zhang[a]

[a]Pennsylvania State University, Dept. of Astrophysics, 525 Davey Lab, University Park, PA 16802

[b]University of Tennessee, Dept. of Nuclear Engineering, Knoxville, TN 37996

ABSTRACT

The Water Recovery X-ray Rocket (WRXR) is a sounding rocket payload that launched from the Kwajalein Atoll in April 2018 and was the first NASA astrophysics sounding rocket payload to be recovered from water. WRXR's primary instrument is a grating spectrometer that consists of a mechanical collimator, X-ray reflection gratings, grazing-incidence mirrors, and a hybrid CMOS detector. We present here the design of the WRXR spectrometer's gratings and mirrors.

Keywords: X-ray, sounding rocket, reflection gratings, off-plane gratings, instrumentation, spectroscopy

1. INTRODUCTION

The Water Recovery X-ray Rocket[1] (WRXR) is a sounding rocket payload that launched from the Kwajalein Atoll in April 2018. An overview of the primary instrument, a soft X-ray grating spectrometer, and its components and science goals was provided in Miles et al. 2017 and a description of a secondary instrument, a lobster-eye hard X-ray imager, was provided in Dániel et al. 2017.[2] The components of the WRXR spectrometer are a mechanical collimator,[3,4] reflection grating array, mirror array, and hybrid CMOS detector.[5,6]

In the WRXR spectrometer, the mechanical collimator collects incident X-rays and sculpts a beam that converges over a 2-meter focal length. Instead of passing through to the focus, light from the collimator is intercepted by an array of X-ray gratings that disperses the incident radiation into a component spectrum. Following the grating array is a co-aligned mirror array that reflects light from the >100-mm long spectral lines produced by the collimator and grating arrays into a more compact area at the focal plane, where a 35 × 35 mm hybrid CMOS detector images the spectrum. In the following sections we will detail design considerations for the spectrometer's gratings and mirrors and present preliminary diffraction efficiency performance of the WRXR gratings.

1.1 X-ray Reflection Gratings

The gratings used in the WRXR spectrometer are off-plane reflection gratings that were designed, fabricated and implemented at Penn State University. Compared to traditional in-plane reflection gratings, off-plane gratings are rotated ∼90° about the grating normal so that the grating facets are approximately parallel to the incident light as shown in Fig. 1. The light is then diffracted in a conical pattern according to the generalized grating equation,[7]

$$sin\alpha + sin\beta = \frac{n\lambda}{dsin\gamma}\,, \tag{1}$$

where γ is the half-cone opening angle between the incident beam and the groove direction, d is the groove spacing, λ is the wavelength of the diffracted light, n is the order number, α represents the azimuthal angle of the reflected light along a cone with half-angle γ, and β is the azimuthal angle of the diffracted light. The gratings in Fig.1b show the Littrow configuration, an orientation in which $\alpha = \beta = \delta$, the grating groove facet angle. In this configuration, specular reflection (called 0 order in the figure) is offset azimuthally by an angle α, and light is preferentially diffracted near the azimuthal angle β in order to maximize throughput as a specific order for a given wavelength.

*dmiles@psu.edu

Space Telescopes and Instrumentation 2018: Ultraviolet to Gamma Ray, edited by Jan-Willem A. den Herder, Shouleh Nikzad, Kazuhiro Nakazawa, Proc. of SPIE Vol. 10699, 106996K · © 2018 SPIE
CCC code: 0277-786X/18/$18 · doi: 10.1117/12.2312648

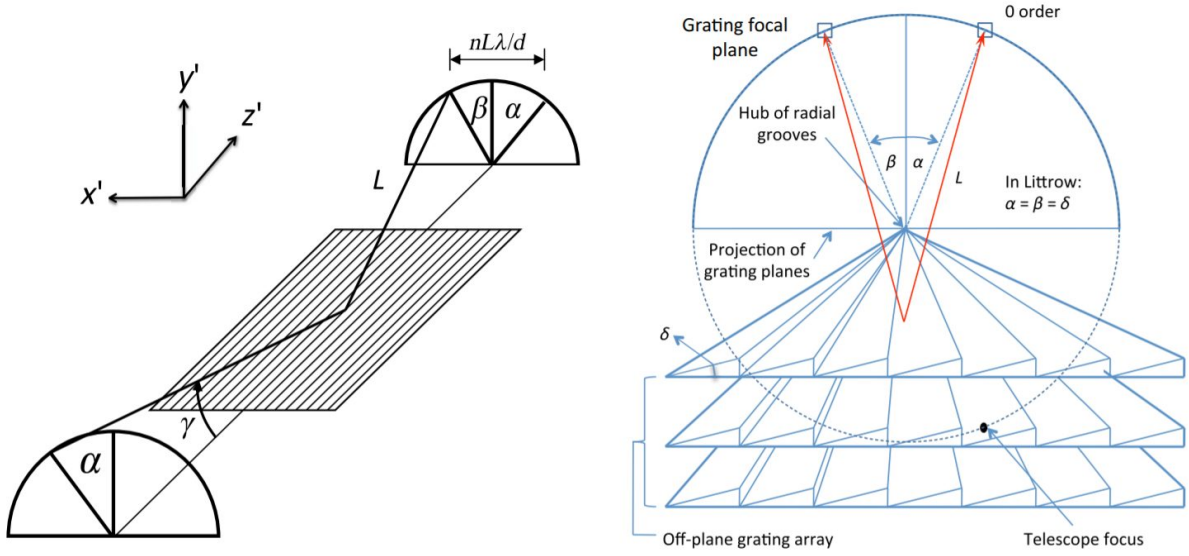

Figure 1. Diffraction geometry of off-plane gratings.[8] (a) At left, light incident quasi-parallel to the groove direction is diffracted into an arc at the focal plane according to Equation 1. The distance L is known as the throw and represents the distance from the grating to the position of the diffracted light on the focal plane. (b) At right, three co-aligned gratings intercept the light that would converge at the focal plane and instead diffract the light onto an arc. In reality, the gratings are separated from the focal plane by several meters, but the image projects the gratings to the focal plane to demonstrate the shared hub and radial convergence. These gratings are placed in the Littrow configuration so that light is preferentially diffracted at the position indicated by the angle β.

2. WRXR GRATING DESIGN

The design of the X-ray reflection gratings for the WRXR spectrometer was driven by science objectives, fabrication limitations, instrument integration capabilities, and development time. Diffraction efficiency is valued more highly than resolving power for WRXR; the resolution of the mechanical collimator is low by grating standards, making it relatively simple to fabricate gratings with a resolving power sufficient to prevent significant grating-induced aberrations to the collimator's LSF. Further, the total on-target time for the WRXR flight was predicted to be ∼4 minutes. Therefore, the primary objective of the WRXR gratings was to maximize diffraction efficiency in the spectral lines of interest while achieving a resolving power sufficient only to prevent significant degradation of the collimator LSF.

The target of the WRXR spectrometer was diffuse soft X-ray emission from the northern half of the Vela supernova remnant. Based on Vela's soft X-ray emission measured by Lu (2000), Moore (1976), and Aschenboch (1994), the WRXR spectrometer was designed to maximize throughput at the OVII triplet (∼21.6 Å[9]), with secondary focus placed on OVIII and CVI.

2.1 Grating Facet Angle

The groove facet angle δ was set by the orientation of the crystal structure in the silicon wafers used for WRXR grating fabrication. Silicon wafers are obtainable at several crystal orientations, and a wafer's underlying crystal orientation determines the orientation of the {111} crystal planes relative to the surface plane.[10] After writing the groove pattern into a resist layer on top of the silicon wafer with an electron-beam lithography (EBL) tool, a series of etches were performed to transfer the groove pattern into the silicon. The process to etch the pattern into the silicon is anisotropic; the silicon etches much more slowly along the {111} plane than the rest of the silicon, resulting in an angled groove defined by the crystal structure and thereby setting the blaze angle of the grating facets. The wafers used for the WRXR spectrometer provided a blaze angle of ∼29.5° and were selected based on wafer availability, the ability to satisfy science requirements, and recent fabrication efforts.[11]

2.2 Grating Dimensions

The physical size of the WRXR gratings was determined by a combination of the physical extent of the collimated beam at the grating location, overall throughput, and flatness concerns. Each grating in the array has a physical size of 100 × 110 mm, where the 110 mm dimension is in the cross-groove direction and is determined by the size of the collimator beam at the position of the grating array, and the 100 mm dimension is set to allow the maximum effective area from a 150 mm wafer (the wafer size used for the WRXR gratings). To maximize geometric throughput, the ideal grating would be infinitely thin; grating thickness presents a cross-section to incident light that is not active grating surface, occulting X-rays from diffracting. In practice, ∼0.5 mm wafers are the thinnest that are easily obtainable while being thick enough to achieve flatness levels that will not negatively affect grating performance. The WRXR gratings were thus designed to be 110 × 100 × 0.5 mm. Based on the size of the collimated beam at the gratings, ∼110 mm of grating coverage is needed, necessitating an array of multiple gratings. For gratings 100 mm long and 0.5 thick, the size of a single grating as seen by incident photons can be found with

$$s = l \sin \eta + t \cos \eta \,, \tag{2}$$

where l is the grating length (100 mm), η is the graze angle, and t is the grating thickness. Considering the apparent size of each grating, ∼4.3 mm for WRXR gratings, and the total grating coverage needed resulted in an array of 26 gratings for the WRXR spectrometer.

2.3 Grating Coating and Graze Angle

With the primary science bandpass determined, the metal used to coat the gratings and provide X-ray reflectivity was studied. Four metals were considered for the WRXR gratings: nickel, iridium, gold, and aluminum. The reflectivity of these materials varies with the angle at which incident photons strike the grating relative to the grating surface, referred to as the graze angle. The geometric throughput of the WRXR grating array also varies with graze; the gratings were imprinted onto silicon wafers that are 100 mm long in the groove direction and ∼0.5 mm thick (refer to §2.2). As the graze angle grows, the apparent size of the grating surface relative to the incident X-rays becomes larger and the thickness of the gratings (which is not an active surface and results in occultation of light) becomes smaller. As a result, geometric throughput (the measure of the fraction of incident photons that strike active grating surface) is larger for higher graze angles. The reflectivity of the metal coatings, however, decreases with increasing graze angle. Both factors were considered in selecting the coating for the WRXR gratings. As shown in Fig. 2, a layer of nickel offers the highest and most stable product of geometric throughput and reflectivity at the primary science wavelength, with peak throughput at a 2.2° graze angle. Based on this information, 2.2° was selected as the nominal graze angle for the WRXR gratings.

The lower limit for the thickness of the nickel layer was determined based on penetration depth of X-rays in the WRXR bandpass; the layer must be thick enough that X-rays will diffract off of the grating coating rather than penetrate to the underlying silicon. The upper limit on nickel thickness must be low enough to preserve the sharp, precise groove facets required for high diffraction efficiency; an excessively thick layer of nickel will cause the groove facets to round off at their peaks. Rounded facets result in a shallower effective blaze angle, causing any X-rays incident on those areas to diffract to lower orders as discussed in §3. Fig. 3 shows one of the WRXR gratings in cross section under a scanning electron microscope (SEM). A layer of nickel can be seen on top of the groove facets, with slight rounding of the features evident. The nickel layer visible in Fig. 3 is ∼20 nm.

2.4 Groove Spacing

At the time of the design for the WRXR gratings, fabrication and testing efforts had been focused on gratings with ∼6000 grooves/mm. Therefore, 6000 grooves/mm was used as a starting point and adjusted based on science goals and detector coverage considerations. Solving Eq. 1 for groove spacing at a specific order for the Littrow configuration yields a groove density of over 10000 grooves/mm for 2nd order OVII, 6790 grooves/mm for 3rd order OVII, and 5032 grooves/mm for 4th order. To provide further constraints on the desired groove density, the linear dispersion of the spectral lines,

$$x = \frac{\lambda n L}{d} \,, \tag{3}$$

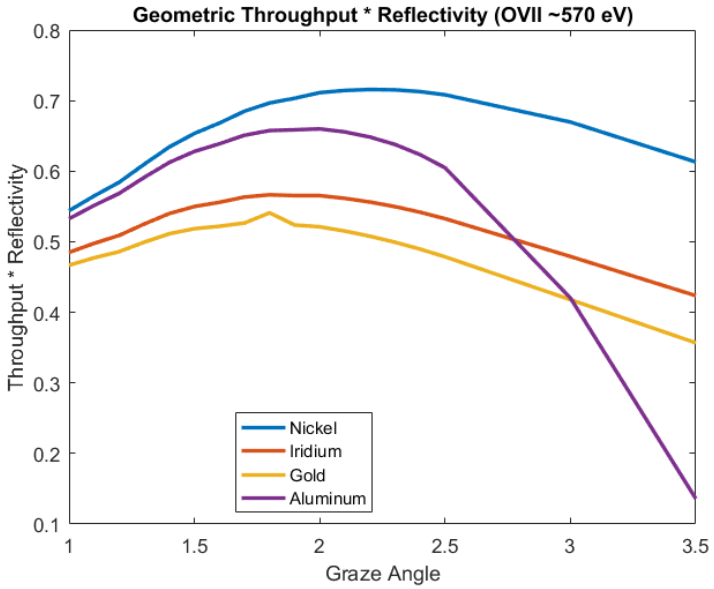

Figure 2. A plot of the combination of geometric throughput of gratings and reflectivity of metal coatings for a range of graze angles. A nickel coating offers the highest overall throughput, with a peak at a graze angle of 2.2°. Reflectivity information was obtained from the Lawrence Berkeley Laboratory's Center for X-ray Optics.

was considered, where λ is wavelength, n is the order number, L is the linear distance from where light is incident on the grating to the given order at the focal plane, and d is the grating groove spacing. Comparing Eq. 3 for two successive orders yields the linear separation between two orders at the focal plane. The linear separation between OVII orders for 10000 grooves/mm is ∼41 mm, the separation for 6790 grooves/mm is ∼28 mm, and that for 5032 grooves/mm is ∼21mm. A dispersion of ∼21mm, combined with a line width of ∼2 mm, allows two orders to fall on the 35-mm detector. While a dispersion of 28 mm for 3rd order optimization would theoretically place two orders on the detector as well, it would impose more strict tolerances on grating alignment and mechanical design. Line separation of ∼41 mm disallows more than a single order of OVII to strike the detector, which removed 10000 grooves/mm from consideration. Placing multiple orders on the detector increases effective area by allowing more photons to strike the detector. With the possibility to place two orders on the detector, the decision was made to optimize for $n = 3.5$. Optimizing to place maximum efficiency between two orders allows mitigation against design and alignment errors; a slight orientation misalignment could cause the peak efficiency to shift to higher or lower orders as the orientation varies from nominal. Capturing multiple orders allows greater opportunity to shift the efficiency to other orders that fall on the detector, rather than orders that are not sampled. Further, optimizing for $n = 3.5$ at OVII also allows diffraction efficiency for CVI to peak near 2nd order and that for OVIII to peak near 4th order (refer to §3 for diffraction efficiency measurements). The resulting groove density was an average of 5750 grooves/mm.

3. PRELIMINARY GRATING EFFICIENCY

To allow for spares and test samples, ∼40 gratings were produced for the WRXR spectrometer. From those 40, 26 were used in the flight grating module and one was randomly selected to take to Lawrence Berkeley National Laboratory's Advanced Light Source (ALS) for efficiency testing. The measurement results are summarized in Fig. 4. The grating test configuration differed slightly from the orientation of the gratings in the flight grating module, resulting in peak diffraction orders being pushed to higher energies. This effect is apparent in Fig. 4, where the intersection between third and fourth orders is seen to be ∼590 eV rather than 570 eV, as designed. Total diffraction efficiency exceeds 70% at low energies and near the CVI emission energy (∼375 eV). Total efficiency at the OVII and OVIII energies (∼570 eV and ∼650 eV, respectively) is above 50%. The cause for the decrease in efficiency above 400 eV is unknown but is possibly due to the rounded features seen in Fig. 3. The

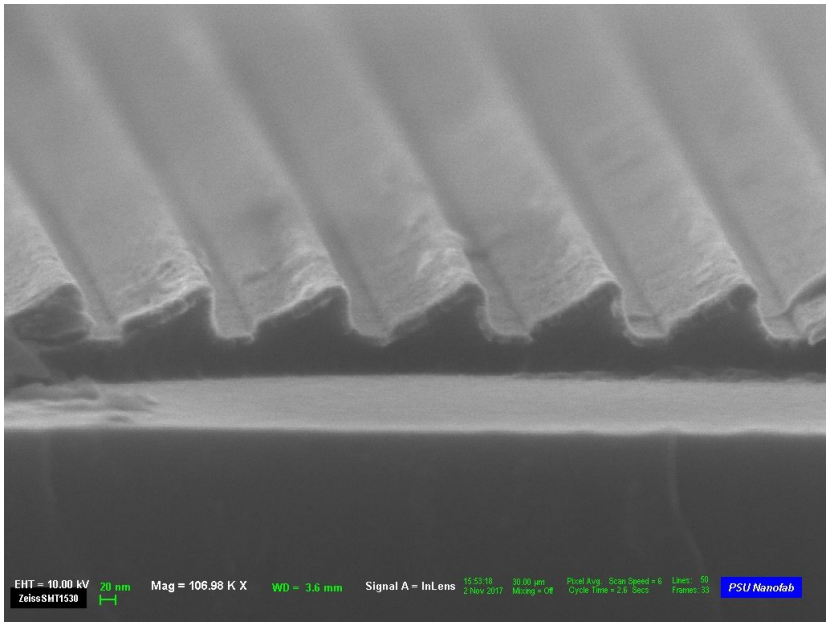

Figure 3. A SEM image of a cross-section of a WRXR grating. A layer of nickel is visible on top of the underlying groove facets. The nickel layer causes the tips of the groove facets to be more rounded, reducing the diffraction efficiency in the blaze envelope.

tail in efficiency seen above 700 eV parallels the dip in reflectivity for Ni at those energies. Further data and analyses are needed to better understand the outlying dip in efficiency at 540 eV.

4. GRAZING-INCIDENCE MIRRORS

The collimated beam of light dispersed by each individual grating is ∼140 mm at the focal plane in the cross-dispersion direction. The 26 gratings in the WRXR spectrometer grating array span a physical distance of ∼110 mm, which produces spectral lines at the focal plane that are >200 mm in cross-dispersion extent. The detector has an active area of 35 × 35 mm, which results in less than 20% of a given spectral line being incident on the detector. One strategy to decrease the cross-dispersion extent of the spectral lines at the focal plane was to co-align each grating so that the hub of each grating points to the same position at the focal plane. However, this technique required that the nominal graze angle of each grating vary from 2.2° for the grating at the center of the array to 2.2° ± ∼0.8° for gratings at the edges of the array. Varying the graze angle of the gratings would require that each grating be aligned into the flight grating module in a unique orientation. Further, the ∼0.8° variation in nominal graze angle would cause a significant decrease to overall diffraction efficiency. Therefore, in order to alleviate alignment concerns and maximize the number of photons that fall on the detector, the gratings were all aligned to the nominal 2.2° graze angle and an array of nickel-coated mirrors were installed after the grating module to reflect the light that would fall outside of the 35 mm detector area onto the detector. The nominal graze angle of each mirror varies based on the desired displacement of the beam at the focal plane; mirrors that reflect light from gratings near the edge of the grating array have a larger graze angle in order to shift the spectral line by a larger distance at the focal plane. Mirrors are less sensitive to the alignment effects of varying graze angles because they reflect any incident light instead of diffracting. However, the distribution of photons in a given spectral line and constraints on mirror alignment disallow a complete recovery of the light that falls outside the detector area. Simulations indicate that the mirror module conservatively allows a factor of ∼1.5 more photons to be collected than the variable-graze method described previously. A schematic diagram of the light path through the collimator, grating array and mirror array is shown in Fig. 5, and the grating and mirror specifications are shown in Table 1.

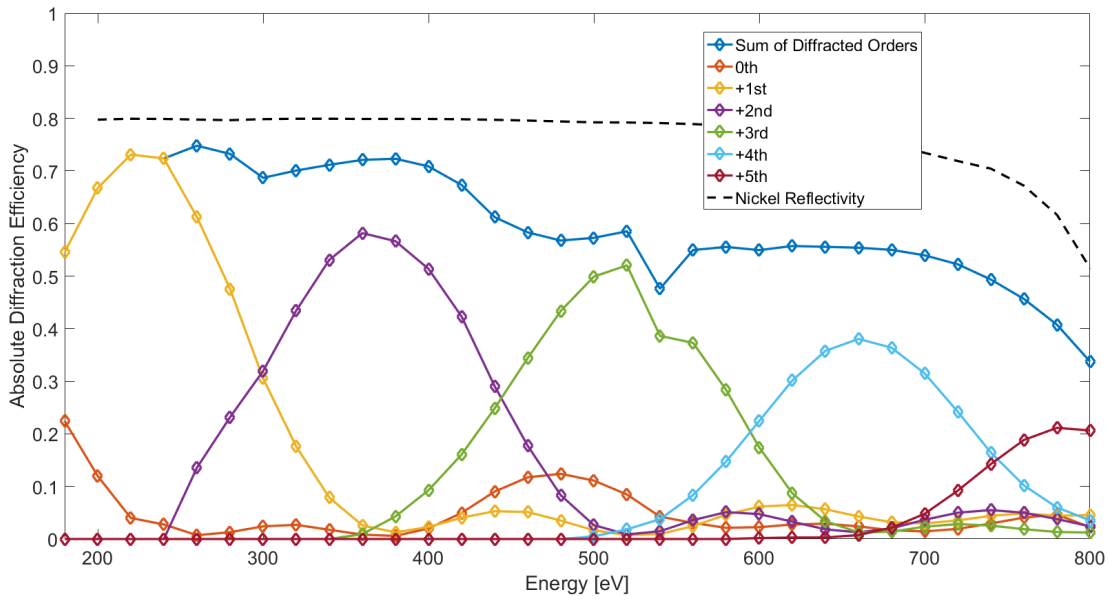

Figure 4. The diffraction efficiency of a grating pulled randomly from the WRXR flight gratings is plotted along with the reflectivity of Ni in the test configuration.

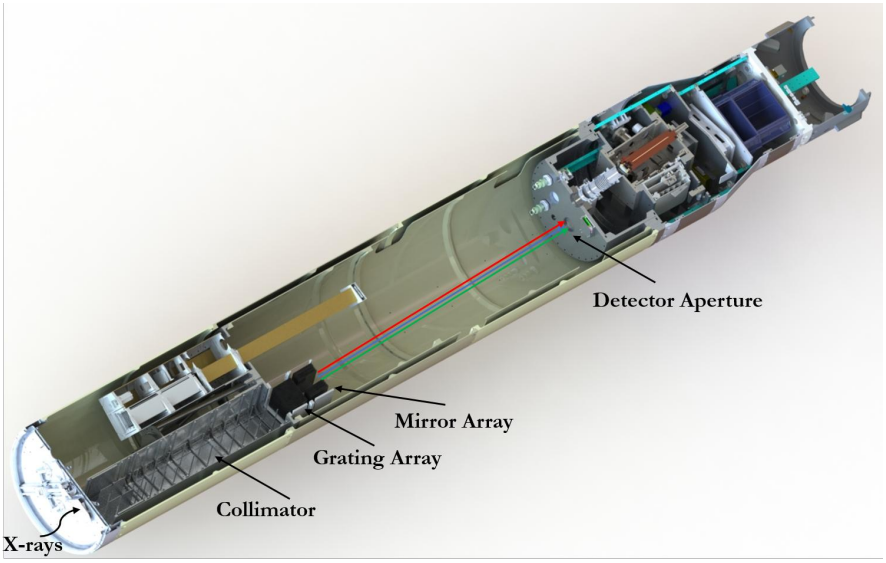

Figure 5. A CAD model of the WRXR payload, with spectrometer components labeled. X-rays are incident from the lower left corner and pass through the mechanical collimator before being diffracted and reflected by the grating array and mirror array, respectively. After dispersing over ∼2 m, the spectrum passes through an open gate valve before being imaged by the detector.

5. SUMMARY AND REMAINING WORK

The WRXR sounding rocket payload launched from the Kwajalein Atoll in April 2018 and was the first NASA astrophysics payload to be recovered from water. The WRXR spectrometer was designed to be sensitive from ∼0.2-0.8 keV, which covers emission lines from CVI up through OVIII, with the primary source of emission from the target source being OVII at 0.57 keV. Preliminary efficiency measurements of the WRXR gratings indicate

Table 1. Specifications for the WRXR gratings and mirrors.

	Gratings	**Mirrors**
Quantity	26	23
Reflective Coating	Nickel	Nickel
Size	110 × 100 × 0.5 mm	110 × 100 × 0.5 mm
Nominal Graze Angle	2.2°	0.35° – 0.80°
Blaze Angle	29.5°	–
Yaw Angle	1.25°	–
Groove Density	5750 grooves/mm	–

∼60% diffraction efficiency in a single order at CVI, ∼55% spread across two orders at OVII, and ∼40% at a single order of OVIII. An array of grazing-incidence Ni-coated mirrors follow the grating array and reflect light from the >100-mm long spectral lines onto a 35-mm long detector at the focal plane.

Future publications will discuss the mass-replication of the WRXR gratings,[17] the alignment and implementation of the WRXR gratings into the instrument,[18] and the flight performance of the payload.

ACKNOWLEDGMENTS

The authors would like to thank the nanofabrication staff at the Penn State Materials Research Institute and Dr. Marc Verschuuren at Philips Innovation Services. The WRXR payload was funded through NASA grants NNX17AD87G and NNX15AC42G.

REFERENCES

[1] Miles, D.M., et al., "An introduction to the Water Recovery X-ray Rocket," Proc. SPIE 10397 (2017).
[2] Dániel, V., et al., "X-ray Lobser Eye all-sky monitor for rocket experiment," Proc. SPIE 10235 (2017).
[3] Zeiger, B.R., "Soft x-ray spectroscopy of the Vela supernova remnant," Doctoral Thesis, University of Colorado (2013).
[4] Rogers, T., McEntaffer, R., Schultz, T., Zeiger, B., Oakley, P., and Cash, W., "The OGRESS sounding rocket payload," Proc. SPIE 885911 (2013).
[5] Hull, S., et al., "Recent X-ray hybrid CMOS detector developments and measurements," Proc. SPIE 10397 (2017).
[6] Falcone, A.D., Burrows, D., Bai, Y., et al., "Hybrid CMOS X-ray Detectors: The Next Generation for Focused X-ray Telescopes," Proc. SPIE 668602 (2007).
[7] Cash, W., "Echelle spectrographs at grazing incidence," Appl. Opt. 21, 710-717 (1982).
[8] McEntaffer, R.L., et al., "First results from a next-generation off-plane X-ray diffraction grating, Experimental Astronomy (2013).
[9] Koutroumpa, D., et al., "OVII and OVIII line emission in the diffuse soft X-ray background: heliospheric and galactic contributions," Astronomy & Astrophysics (2007).
[10] DeRoo, C.T., et al., "Line spread functions of blazed off-plane gratings operated in the Littrow mounting," Journal of Astronomical Telescopes, Instruments, and Systems 2(2), 025001 (2016).
[11] Miles, D.M., et al., 'Fabrication and diffraction efficiency of a replicated X-ray reflection grating," in prep (2018).
[12] Seely, J.F., et al., "Efficiency of a grazing-incidence off-plane grating in the soft-x-ray region," Appl. Opt. 45, 1680-1687 (2006).
[13] McEntaffer, R.L., et al., "First results from a next-generation off-plane X-ray diffraction grating," Experimental Astronomy 36, Issue 1-2, pp 389-405 (2013).

[14] DeRoo, C.T., et al., "Line Spread Functions of Blazed Off-Plane Grating Operated in the Littrow Mounting," Journal of Astronomical Telescopes, Instruments, and Systems 2, 025001 (2016).
[15] Donovan, B.D., et al., "X-ray verification of an optically aligned off-plane grating module," Appl. Opt. 57, 454-464 (2018).
[16] Cash, W.C., "X-ray spectrographs using radial groove gratings," Appl. Opt. 22, 3971-3976 (1983).
[17] McCoy, J., et al., "X-ray reflection grating replication using substrate conformal imprint lithography," In prep (2018).
[18] Tutt, J.H., et al., "X-ray reflection grating alignment for the Water Recovery X-ray Rocket," In prep (2018).